Introduction

X-ray astronomy was born in the aftermath of World War II as military rockets were repurposed to lift radiation detectors above the atmosphere for a few minutes at a time. These early flights detected and studied X-ray emission from the solar corona. The first sources beyond the Solar System were detected during a rocket flight in 1962 by a team headed by Riccardo Giacconi at American Science and Engineering, a company founded by physicists from MIT. The rocket used Geiger counters with a system designed to reduce non-X-ray backgrounds and collimators limiting the region of sky seen by the counters. As the rocket spun, the field of view (FOV) happened to pass over what was later found to be the brightest non-solar X-ray source, later designated Sco X-1. It also detected a uniform background glow which could not be resolved into individual sources. A follow-up campaign using X-ray detectors with better spatial resolution and optical telescopes identified Sco X-1 as an interacting binary with a compact (neutron star) primary.

This success led to further suborbital rocket flights by a number of groups. More X-ray binaries were discovered, as well as X-ray emission from supernova remnants, the radio galaxies M87 and Cygnus-A, and the Coma cluster. Detectors were improved and Geiger counters were replaced by proportional counters, which provided information about energy spectra of the sources. A constant challenge was determining precise positions of sources as only collimators were available.

The first X-ray astronomy satellite, Uhuru, was developed by Giacconi's team and launched by NASA in 1970. In its first day it exceeded the combined observation time of all previous X-ray astronomy experiments. Uhuru performed an all-sky survey using collimated proportional counters and detected over 300 individual sources. Among the discoveries from Uhuru were pulsations from X-ray binaries and extended X-ray emission from clusters of

galaxies. The 1970s saw a succession of increasingly sophisticated satellites with X-ray detectors. Among them were Copernicus, Ariel-V (from the UK), ANS (from the Netherlands), OSO-8, and HEAO-1. These missions established further classes of astronomical objects as X-ray sources, observed more types of time variability from X-ray binaries, and detected iron emission lines.

The next revolution in X-ray astronomy was wrought by the Einstein Observatory, launched in 1979 and named in honour of the centenary of his birth. X-ray focusing optics had been flown on Copernicus and as part of the solar astronomy experiment on Skylab but the Einstein Observatory provided the first X-ray images of many classes of astronomical objects. The combination of an X-ray telescope and an imaging proportional counter provided the sensitivity to observe large samples of stars, binaries, galaxies, clusters of galaxies, and active galactic nuclei (AGN). In addition, the focusing optics allowed the use of physically small detectors such as solid-state and crystal spectrometers as well as a grating that dispersed the spectrum onto a microchannel plate detector. The Einstein Observatory was one of the first astronomy satellites to have a guest observer program. Another innovation was an automated data-reduction pipeline and a public archive. Although this pre-dated the Internet, and thus required actual travel to the archive, it was an important first step.

The 1980s were a lean period for X-ray astronomy in the USA but progress continued in Europe and Japan. Exosat was launched by ESA in 1983 into a deep 90-hour-period orbit which allowed long, continuous observations of sources. The Japanese scientific space agency, ISAS, pursued a program of placing mainly large-area proportional and scintillation counters on a series of satellites: Hakucho, Tenma and Ginga. Among the discoveries in this decade were quasi-periodic oscillations (QPOs) in X-ray binaries, iron emission and absorption lines from AGN and iron emission lines from the Galactic center. The successor to the Einstein Observatory was ROSAT, a German–US–UK collaboration with X-ray and extreme ultraviolet (EUV) telescopes, which was launched in 1990. The first six months were spent performing an all-sky survey, generating a catalog of more than 150 000 objects, followed by another eight years of targeted observations as part of a guest observer program, accumulating another catalogue of 100 000 serendipitous sources. ROSAT was able to image over a two-degree FOV providing good observations of large supernova remnants, clusters of galaxies, structure in the interstellar medium, and comets.

The next big technological advance was the use of X-ray-sensitive charge-coupled devices (CCDs), which provide better imaging and spectroscopic

properties than imaging proportional counters or scintillators. ASCA, launched in 1993 and a collaboration between ISAS and NASA, was the first X-ray astronomy satellite carrying CCDs. ASCA's other innovation was light-weight optics which provided a much larger area than those used for ROSAT although with poorer spatial resolution. The light-weight optics were placed in an extendable structure giving a long enough focal length to take the ASCA bandpass up to 10 keV, thus including the important 6–7 keV iron line region. This improvement enabled the detection and study of relativistically broadened iron lines in the accretion disks around black holes. Another major discovery made possible by the broad energy bandpass was that of non-thermal X-ray emission in supernova remnants.

While most X-ray satellites now use focusing optics, there is still a place for large-area proportional counters. RXTE, launched by NASA in 1996, was designed to collect many events from bright sources and to examine their variability down to microsecond timescales. An all-sky monitor tracked the brightest sources on day to year timescales. Among RXTE's discoveries were spin periods in low-mass X-ray binaries and kilohertz QPOs. RXTE's all-sky monitoring duties have now been taken over by the Japanese MAXI detector on the International Space Station.

In recent years, X-ray observations of gamma-ray bursts have become important. The Italian–Dutch satellite BeppoSAX, launched in 1996, had two sets of detectors. Proportional counters behind coded aperture masks were used to detect gamma-ray bursts and determine their approximate positions. These positions were used by ground controllers to point a set of narrow-field detectors at the source to observe the X-ray afterglow. This strategy was improved upon by the NASA satellite, Swift, launched in 2004, which autonomously points its X-ray and UV/optical telescopes at bursts detected by its wide-field coded aperture mask camera.

We are now in the era of great observatories with Chandra from NASA, XMM–Newton from ESA, and Suzaku from JAXA, all operational. Chandra's strength is its sub-arc second resolution telescope giving high-resolution images and, using gratings, spectra. XMM–Newton has the largest area of any focusing X-ray telescope while Suzaku covers a wider energy bandpass and has the lowest background. In the next few years, a number of other X-ray astronomy missions are planned. From NASA, NuSTAR will use focusing optics at energies above 10 keV for the first time and GEMS will measure X-ray polarization. A collaboration between Russia and Germany, Spectrum–Roentgen–Gamma, will perform a new, more sensitive, all-sky survey. Astro-H, the next JAXA mission, done in collaboration with NASA, will feature a microcalorimeter providing sensitive, non-dispersive, high-resolution spectroscopy. The

international basis of X-ray astronomy is expanding as India, China, and Brazil all prepare their own satellites.

After its first half-century, observations in the X-ray waveband have become important in many topics in astronomy. Despite this, its techniques remain unfamiliar to many astronomers. One reason is that X-rays are almost always detected event by event instead of as a bolometric flux over a specific bandpass, as is common in other wavebands. However, the differences are not just in detection methods. While optical spectroscopy is concerned principally with line emission and absorption and radio spectroscopy with continuum emission, the processes that generate X-rays create significant continuum as well as line emission and both must be modelled correctly. Complicating this further, until recently, X-ray detectors did not have the spectral resolution needed to separate the lines from the continuum cleanly.

These and other issues have continued to make X-ray data analysis challenging. Following the launch of Chandra and XMM–Newton, the need for more systematic training of graduate students interested in X-ray astronomy became clear, leading to a series of X-ray "schools." These schools have been organised in the USA by the Chandra X-ray Center (CXC) and NASA Goddard Space Flight Center (GSFC), in Europe by the XMM–Newton Science Operation Centre (SOC), and in the developing world by the COSPAR Capacity-Building Workshop program. All of the authors of this handbook have lectured at these schools, in most cases multiple times, and the material collected here was developed through interactions with the students at the schools.

We have attempted to steer a middle course between pure theoretical exposition and explicitly detailing commands, albeit with excursions to both sides. We hope that this handbook proves to be a useful guide to beginning X-ray astronomers as well as experienced scientists who need to remember a conversion factor. To that end, we have arranged the text in three sections. The first three chapters cover the optics and detectors used on X-ray satellites. The next five chapters describe analysis issues, including data preparation, calibration, and modelling. Finally, the appendices contain a range of useful tables, including atomic data, conversion factors, and typical X-ray sources, amongst other information.

The editors thank Ilana Harrus for laying the initial groundwork for this book and Peter Wilmore for organizing the COSPAR workshops which provided much of our inspiration. We thank Adam Foster for creating a figure for Chapter 5, John Vallerga for help with Appendix 2 and Ken Ebisawa for help with Appendix 4. Nancy Brickhouse, Andrew Szentgyorgyi,

Harvey Tananbaum, Panayiotis Tzanavaris and Martin Zombeck provided helpful comments on the draft. The section on timing analysis leans heavily on X-ray astronomy talks given by Michael Nowak and Tod Strohmayer although they bear no responsibility for any errors introduced. Last, but not least, we thank our spouses for putting up with our distraction while finishing this book.

1

Optics

DANIEL A. SCHWARTZ

1.1 Introduction

It may be obvious why visible astronomy utilizes images, but it is illustrative to consider the value of focusing to X-ray astronomy. A list of advantages offered by the best possible two-dimensional angular resolution would include:

(i) Resolving sources with small angular separation and distinguishing different regions of the same source.
(ii) Using the image morphology to apply intuition in choosing specific models for quantitative fits to the data.
(iii) Using as a "collector" to gather photons. This is necessary because X-ray-source fluxes are so low that individual X-ray photons are detected; the weakest sources give less than one photon per day.
(iv) Using as a "concentrator," so that the photons from individual sources interact in such a small region of the detector that residual non-X-ray background counts are negligible.
(v) Measuring sources of interest and simultaneously determining the contaminating background using other regions of the detector.
(vi) Using with dispersive spectrometers such as transmission or reflection gratings to provide high spectral resolution.

The Earth's atmosphere completely absorbs cosmic X-rays. Consequently, X-ray observatories must be launched into space; so size, weight, and cost are always important constraints on the design. In practice this leads to a trade-off between the best possible angular resolution and the largest possible collecting area.

Realizing an X-ray telescope involves two key issues: reflection of X-rays, and formation of an image. We discuss each in turn.

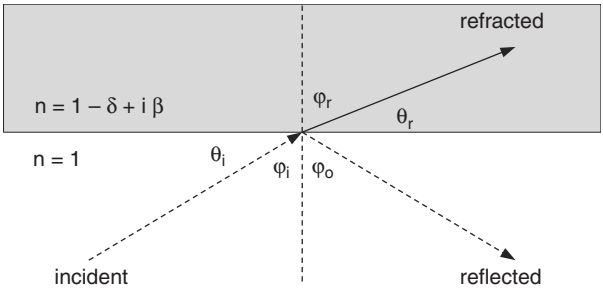

Fig. 1.1 An X-ray in the vacuum (unshaded lower region) impacts a medium (shaded upper region) at a grazing angle θ_i. When the real part of the index of refraction, $1–\delta$, is less than 1, the refracted angle θ_r is smaller than the grazing angle. Since $\cos\theta_r$ cannot be larger than 1, there is total external reflection for grazing angles less than $\arctan(1-\delta)$

1.2 X-ray reflection

X-rays incident on a material will, in general, penetrate and, if the material is thick enough, be absorbed. This is the basis of their utility in familiar applications such as medical diagnosis and luggage inspection. However, when impacting a surface at small grazing angles X-rays can reflect. An analogy is skipping stones on water instead of dropping them straight in. For X-rays the physical process is total external reflection, in which an individual photon collectively interacts with an ensemble of surface electrons. It is scattered coherently only in a special direction; namely, in accordance with the familiar law for all optical reflection, that the angle of incidence equals the angle of reflection, $\phi_i = \phi_o$.

1.2.1 Total external reflection

Figure 1.1 shows the interaction between an incident ray in the vacuum and a solid medium. The medium has an index of refraction $n = 1 - \delta + i\beta$, where δ and β are the optical constants (tabulated in e.g. Henke *et al.*, 1993). Both optical constants are very much smaller than unity in the X-ray regime. They are proportional to the square of the wavelength and the real and imaginary parts of the complex atomic scattering factor. If the medium is conductive then β is non-zero and the refracted ray will decay exponentially.

The incident and refracted angles are related by Snell's law:

$$\sin\phi_r = \sin\phi_i/(1-\delta) \tag{1.1}$$

In X-ray optics applications it is conventional to use the grazing angle $\theta = \pi/2 - \phi$ measured relative to the tangent to the surface. Snell's law is then:

$$\cos\theta_r = \cos\theta_i/(1-\delta) \tag{1.2}$$

Total reflection occurs when there is no real solution for θ_r in Equation 1.2. At X-ray wavelengths the optical constant δ is always positive so, since $\cos\theta_r$ cannot exceed unity, there is a critical grazing angle θ_c below which refraction is impossible and total external reflection occurs. The angle θ_c is given by $1 = \cos\theta_r = \cos\theta_c/(1-\delta)$, or $\cos\theta_c = (1-\delta)$. For small angles $1 - \delta = \cos\theta_c \approx 1 - \theta_c^2/2$ so that $\theta_c = \sqrt{2\delta}$.

At X-ray energies, E, which are not too near absorption edges of the reflecting material, the optical constant δ is given by:

$$\delta = r_e(hc/E)^2 N_e/(2\pi) \tag{1.3}$$

where r_e is the classical electron radius, N_e the electron density, h Planck's constant and c the speed of light. Since N_e is proportional to the atomic number Z the critical grazing angle can be written:

$$\theta_c \propto \sqrt{Z}/E \tag{1.4}$$

Thus, the critical angle decreases inversely proportionally to the energy. Higher-Z materials are desireable for reflecting surfaces since they have a larger critical angle at any energy and will reflect at higher energies at any fixed grazing angle.

The above discussion must be modified for energies just above atomic edges where absorption coefficients increase and reflectivity decreases. It is important to verify calculations experimentally in these energy ranges during calibration and bear in mind during data analysis that there may be additional systematic uncertainties.

The grazing angle will typically define the maximum angular size of the FOV. Current-generation X-ray telescopes typically have energy ranges from 0.1 to 10 keV using grazing angles of 1/2 to 1 degree. Materials such as gold, platinum, and iridium are good reflectors for these energy ranges. Lighter-weight materials such as beryllium, aluminum, and nickel were used in earlier telescopes designed for X-rays with energies primarily below 1 keV.

1.2.2 The Fresnel equations and reflectivity

After determining the conditions for reflection it remains to calculate the amplitude. Assuming a plane wave incident from vacuum onto an infinitely smooth surface then the components of $E_\parallel$, $H_\parallel$, $D_\perp$ and $B_\perp$ must be continuous across

the interface (Jackson, 1988). Maxwell's equations then give the Fresnel equations:

$$r_{\rm p} \equiv \frac{(n^2\ \sin\theta - (n^2 - \cos^2\theta)^{1/2})}{(n^2\ \sin\theta + (n^2 - \cos^2\theta)^{1/2})} \tag{1.5}$$

$$r_{\rm s} \equiv \frac{(\sin\theta - (n^2 - \cos^2\theta)^{1/2})}{(\sin\theta + (n^2 - \cos^2\theta)^{1/2})} \tag{1.6}$$

where $r_{\rm p}$ is for the parallel component (i.e. in the plane of the incident and reflected photon) and $r_{\rm s}$ for the perpendicular component of the electric vector. The squared amplitudes of the complex numbers $r_{\rm p}$ and $r_{\rm s}$ are the reflectivities of each component. For unpolarized X-rays the desired reflectivity is just:

$$R = (\mid r_{\rm p} \mid^2 + \mid r_{\rm s} \mid^2)/2 \tag{1.7}$$

Since the squared amplitude of the refraction index, n^2, is very nearly unity in the X-ray range, polarization can be generally ignored and Equation 1.7 used for the reflectivity of a single surface. The high accuracy of this assumption is very convenient for designing a mirror, but has the unfortunate consequence that the measurement of X-ray polarization is very difficult.

1.2.3 X-ray reflection in practice

For the practical design, calibration, and analysis of data from X-ray telescopes, at least three other significant effects must be considered: scattering; interface of the mirror surface to the X-ray incident in vacuum; and preparation of the reflecting surface.

Surfaces are not infinitely smooth, as assumed in applying the boundary conditions for calculating the Fresnel equations. A bumpy surface will scatter incident X-rays. This scattering cannot be treated exactly because it is caused by deviations of a few Ångstrom on linear scales of a micrometer and less, which cannot be measured. Section 1.3.3 describes how to calculate scattering using a statistical description of the surface roughness. The key features to remember are that scattering is proportional to E^2, and that scattering in the plane defined by the surface normal and incident X-ray direction dominates over out-of-plane scattering by a factor $1/\sin\theta$.

The interface from a vacuum to a single, infinitely thick reflecting layer is thus an oversimplification. There typically is a substrate material which is formed and polished to the figure required for optical performance. For Chandra this is Zerodur, a special glass with an extremely small coefficient of thermal expansion. The high-Z metal which provides the high reflectivity is deposited on this substrate. However, materials such as gold or iridium require a binding

layer, e.g. chromium, to hold the metal to the glass. Finally, there is an unwanted but unavoidable overcoat of molecular contaminants (e.g. carbon, oxides, . . .). At those energies where the reflectivity of the heavy metal is not near unity, i.e. high energies, large grazing angles, and above atomic edges, the X-ray penetrates the metal, so that the additional layers have a significant effect. One consequence is that reflectivity at some energies can be enhanced due to constructive interference from the different layers. This has been exploited to construct multi-layer mirrors for high-energy X-rays and for near-normal incidence mirrors at energies below 1 keV (see Section 1.3.5).

The index of refraction, and hence the Fresnel equations, assume the ideal density of a bulk material. However, the thin layers of reflecting metal, typically only a few hundred Ångstroms thick, do not necessarily have such a high density. Why not make a mirror out of pure gold? Aside from the cost of gold, it is a soft material with a relatively high coefficient of thermal expansion, which would not preserve a shape to the required specification under practical conditions. Also, since the weight that can be launched into space is a crucial limitation, a thick, high-density material would only allow very small mirrors. The density of the reflecting layer depends on the method of deposition. Sputtering generally results in a higher density than evaporative heating and deposition.

1.3 X-ray mirrors

Now that we understand how X-rays reflect, we can consider how to form surfaces which will bring an incident bundle of parallel rays to as close a point image as possible in the focal plane. X-ray astronomy studies sources such as supernova remnants, galaxies, and clusters of galaxies, which have sizes of many arc minutes, so focusing should be performed over a FOV of at least this extent. We consider first a simple parabola, and then the paraboloid and hyperboloid shapes, which have been the standard configuration for cosmic X-ray astronomy imaging.

1.3.1 Parabolas

Photons incident parallel to the axis of a parabola will all be reflected to converge at its focus. To verify this, consider that an incoming ray will hit the parabola at an angle $\alpha = \arctan \mathrm{d}R/\mathrm{d}z$ and be diverted through an angle 2α to follow a line defined by the equation $\tan 2\alpha = R/(z - f)$, where f is the distance from the origin to the focus, z is the coordinate along the parabola